ChemComm

COMMUNICATION

View Article Online
View Journal | View Issue

Cite this: *Chem. Commun.*, 2020, **56**, 7589

Received 17th February 2020,
Accepted 1st June 2020

DOI: 10.1039/d0cc01161d

rsc.li/chemcomm

Binding modes of thioflavin T and Congo red to the fibril structure of amyloid-β(1–42)†

Benedikt Frieg, [ab] Lothar Gremer, [bc] Henrike Heise, [bc] Dieter Willbold [bc] and Holger Gohlke *[abd]

Binding modes for the amyloid-β(1–42) fibril fluorescent dyes thioflavin T and Congo red were predicted by molecular dynamics simulations and binding free energy calculations. Both probes bind on the fibril surface to primarily hydrophobic grooves, with their long axis oriented almost parallel to the fibril axis. The computed binding affinities are in agreement with experimental values. The binding modes also explain observables from previous structural studies and, thus, provide a starting point for the systematic search and design of novel molecules, which may improve *in vitro* diagnostics for Alzheimer's disease.

Alzheimer's disease (AD) is a progressive, unremitting, neurodegenerative disorder.[1–4] In 2018 it was assumed that more than 50 million people worldwide are living with dementia, with two-thirds associated with AD. Recent estimates assume that by 2030 more than 80 million people will be diagnosed with dementia.[5,6] The considerable number of dementia patients will incur high costs for the healthcare system, which are predicted to rise to worldwide $2 trillion by 2030.[6] Thus, dementia and AD, in particular, constitute serious challenges for the modern healthcare system.

AD is related to the production–elimination-imbalance of the peptide amyloid-beta (Aβ).[7] At high concentration, Aβ peptides tend to aggregate to oligomers or arrange to symmetric, periodic fibrils, both denoting pathological hallmarks in AD.[4,7–9] One diagnostic strategy focuses on detecting biomarkers for AD,[5,6] such as the accumulation of Aβ fibrils.[5,6] As changes in the brain begin 20 years or more before AD-related symptoms are expected to occur,[5,6] a conclusive test will be essential. This is all the more true as a therapeutic intervention in the very early stages of AD is currently considered necessary to stop its progression.[5,6] Fluorescent dyes that detect Aβ fibrils, for example, thioflavin T (THT) and Congo red (CR)[10,11] (Fig. S1, ESI†), are thus essential for an accurate and conclusive diagnosis.

THT and CR form fluorescent complexes with amyloid and amyloid-like fibrils.[12–14] For both probes, previous studies suggested binding modes,[10,11,15] but the exact nature of how the probes bind to the Aβ(1–42) fibril remained elusive. Such knowledge is, however, essential for the systematic search for novel molecular probes.[10,11] The recent success in structure determination of the Aβ(1–42) fibril[16] offers the possibility to predict the binding modes of THT and CR to that fibril.

We applied all-atom molecular dynamics (MD) simulations of free THT and CR diffusion in the presence of the Aβ(1–42) fibril of an aggregate time of 45 μs to derive such binding modes. The simulations were not biased by any prior information on potential binding epitopes. Over simulation times of 1 μs, THT repeatedly binds to and unbinds from the fibril (Fig. S2 and Movie S1, ESI†). CR, by contrast, does not unbind completely but moves across the fibril surface once bound (Fig. S3 and Movie S2, ESI†), suggesting that CR binds with higher affinity.

To identify the most likely binding epitopes, we computed probability densities of the location of either dye. THT predominantly binds in the vicinity of V18, F20, and E22 on either protofilament (Fig. 1A). For CR, by contrast, multiple areas are identified across the fibril surface (Fig. 2A). Likely, this is because CR can form hydrophobic, ionic, and hydrogen bond interactions, enabling binding to different sites. The vicinity of V18, F20, and E22, however, is weakly occupied by CR, suggesting that both probes bind to distinct epitopes. Stably bound conformations (Fig. S4, ESI†) were clustered to extract the most relevant binding poses. The ten largest clusters were

[a] *John von Neumann Institute for Computing (NIC), Jülich Supercomputing Centre (JSC), Forschungszentrum Jülich GmbH, Jülich, Germany*
[b] *Institute of Biological Information Processing (IBI-7: Structural Biochemistry), Forschungszentrum Jülich GmbH, Jülich, Germany*
[c] *Institut für Physikalische Biologie, Heinrich Heine University Düsseldorf, Düsseldorf, Germany*
[d] *Institute for Pharmaceutical and Medicinal Chemistry, Heinrich Heine University Düsseldorf, Düsseldorf, Germany. E-mail: gohlke@uni-duesseldorf.de*

† Electronic supplementary information (ESI) available: Detailed instructions for system preparation, simulations, and analysis procedures, and results from RMSD measurements, clustering, and binding affinity computations, additional binding poses, and force field parameters for CR. The supplemental movies show representative MD trajectories of THT (Movie S1) and CR (Movie S2) binding. See DOI: 10.1039/d0cc01161d

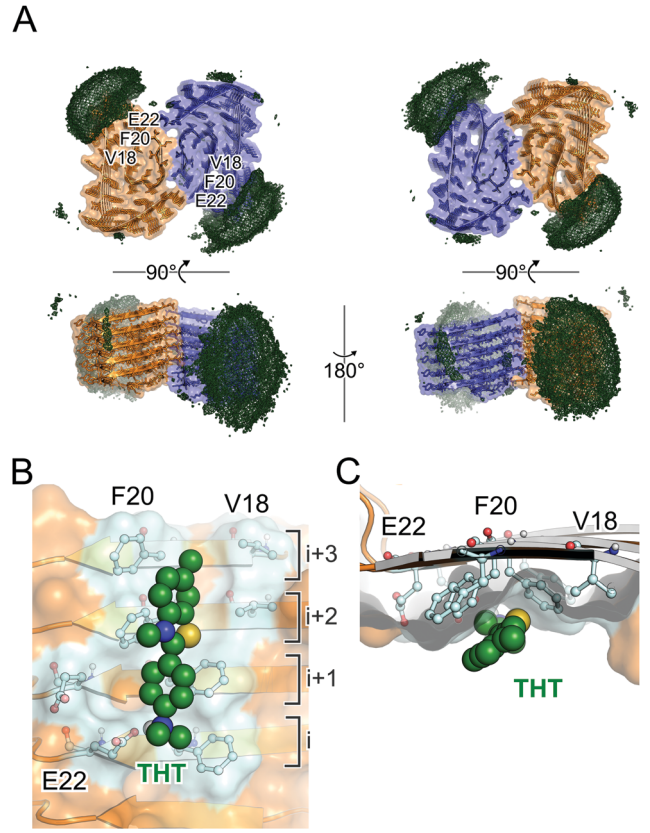

Fig. 1 (A) 3D density grids representing the probability density of the thioflavin T (THT) position around the Aβ(1–42) fibril (blue-orange cartoon-surface representation). (B and C) Predominant THT binding pose (sphere representation) from the c0 cluster in side (B) and top-view (C), with amino acids (cyan ball-stick model) binding THT.

further subjected to molecular mechanics generalized Born surface area (MM-GBSA)[17] and normal mode analysis (NMA)[18] calculation, yielding $\Delta G^0_{\mathrm{bind}}$ (eqn (S1)–(S3), ESI†). Although the MM-GBSA method is established as a fast and reliable method to estimate effective binding energies, considering the entropic contributions by NMA may introduce some uncertainty.[19,20] In the present study, however, the MM-GBSA and NMA calculations were performed on pre-clustered sets of dye poses, such that the total error (eqn (S6), ESI†) for most THT cluster is <1.0 kcal mol^{-1} and for CR cluster is <1.5 kcal mol^{-1} (Tables S1 and S2, ESI†) and, thus, comparable to the uncertainty of more rigorous, but computationally less efficient methods.[21] From $\Delta G^0_{\mathrm{bind}}$ we derived the dissociation constant $K_{\mathrm{D}}^{\mathrm{comp}}$ (eqn (S4), ESI†) for each cluster. Focusing on the interpretation of $K_{\mathrm{D}}^{\mathrm{comp}}$ and its upper and lower limits, we derive binding mode models that are in agreement with previous observables.

Experimental binding affinities ($K_{\mathrm{D}}^{\mathrm{exp}}$) of THT to Aβ(1–42) fibrils range from 294–4000 nM.[22,23] We identified three THT clusters the configurations of which yield $K_{\mathrm{D}}^{\mathrm{comp}}$ in excellent to very good agreement with $K_{\mathrm{D}}^{\mathrm{exp}}$ (Table S1, ESI†). The c0 cluster results in the most favorable affinity ($\Delta G^0_{\mathrm{bind}} = -9.06 \pm 0.42$ kcal mol^{-1}, $K_{\mathrm{D}}^{\mathrm{comp}}$ = 113–470 nM, Table S1, ESI†), followed by c3 ($\Delta G^0_{\mathrm{bind}} = -8.37 \pm 0.52$ kcal mol^{-1}, $K_{\mathrm{D}}^{\mathrm{comp}}$ = 305–1759 nM, Table S1, ESI†), and c1 ($\Delta G^0_{\mathrm{bind}} = -8.14 \pm 0.45$ kcal mol^{-1}, $K_{\mathrm{D}}^{\mathrm{comp}}$ = 506–2331 nM, Table S1, ESI†). The intramolecular mobility of THT is reduced in the bound conformation (Fig. S5, ESI†), which is a structural prerequisite for a dye to fluoresce.[24] THT configurations of these clusters bind to V18, F20, and E22, with THT's protonated amino function forming a salt bridge with E22, and F20 and V18 accommodating the aromatic moieties (Fig. 1B, C and Fig. S6, ESI†). In doing so, the side chains of F20 adopt a V-shaped orientation, forming π–π-stacking interactions with the aromatic rings in THT. THT binds across multiple Aβ(1–42) peptides with its axis oriented almost perpendicularly to the orientation of the stacked β-strands. The observation provides an explanation of why THT recognizes fibrillary structures but no single Aβ(1–42) peptides.[25,26]

$K_{\mathrm{D}}^{\mathrm{exp}}$ values of CR to Aβ(1–42) fibrils range from 209–3070 nM.[27] We identified two CR clusters the configurations of which yield $K_{\mathrm{D}}^{\mathrm{comp}}$ in excellent agreement with experiments (Table S2, ESI†). The c3 cluster results in the more favorable binding affinity ($\Delta G^0_{\mathrm{bind}} = -11.07 \pm 1.31$ kcal mol^{-1}, $K_{\mathrm{D}}^{\mathrm{comp}}$ = 0.84–70 nM, Table S2, ESI†) than the c7 cluster ($\Delta G^0_{\mathrm{bind}} = -9.78 \pm 1.82$ kcal mol^{-1}, $K_{\mathrm{D}}^{\mathrm{comp}}$ = 3–1458 nM, Table S2, ESI†). The intramolecular mobility in the bound conformation is reduced markedly in the central biphenyl group and to some extent across the diazen moiety (Fig. S7, ESI†). CR binds to the groove between Y10 and V12, forming edge-to-face aromatic and hydrophobic interactions between its almost planar biaryl core with Y10 and V12, respectively. CR also forms hydrogen bonds with the backbone carbonyl oxygen of E11, while the sulfonic acid and sulfonate groups are solvent-exposed (Fig. 2B, C and Fig. S8A, ESI†). CR binds across six layers of Aβ(1–42) peptides with its axis oriented almost perpendicularly to the orientation of the stacked β-strands of the Aβ fibril. In one simulation, CR intercalates into the protofilament (Fig. S8B, ESI†), with $\Delta G^0_{\mathrm{bind}} = -14.38 \pm 1.95$ kcal mol^{-1} and $K_{\mathrm{D}}^{\mathrm{comp}}$ = 0.001–0.79 nM (Table S2, ESI†). However, this pose was only observed in one of 45 simulations, suggesting that it is the consequence of a kinetic trapping rather than a thermodynamically favorable binding.

The reported binding epitopes and modes for THT and CR agree with experimental observables on multiple accounts. First, the differences in the occurrence frequencies of THT in the vicinity of amino acids V18, F29, and E22 (Fig. 1) and CR across the entire surface of the Aβ(1–42) fibril (Fig. 2) are in line with *in vitro* data suggesting that THT-type ligands and CR-type ligands bind to distinct, non-overlapping sites on Aβ aggregates: one type could not be replaced by the other when bound to Aβ aggregates.[23] Second, the binding stoichiometry of CR to insulin fibrils is ~20-fold higher than of THT, suggesting that there are likely more binding sites for CR,[11] which agrees with our observation that CR tends to bind to the entire fibril surface. By contrast, in early studies on CR binding to amyloid fibrils, a single binding site was identified only.[28] Recent high-resolution structures of amyloid fibrils[16,29–32] revealed highly symmetric and periodic complexes, however, supporting the view of multiple, identical binding sites. Luminescent-conjugated oligothiophene biomarkers were also shown to bind concurrently to the fibril.[33]

THT is predicted to bind to V18, F20, and E22 on the fibril surface. The fast kinetics of THT binding to fibrils suggests that

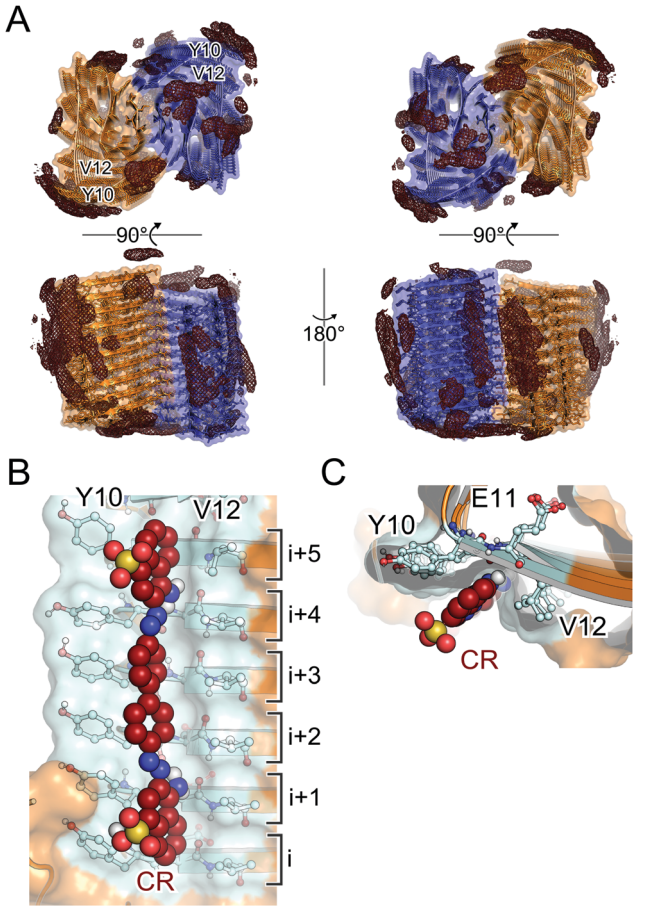

Fig. 2 (A) 3D density grids representing the probability density of the Congo red (CR) positions around the Aβ(1–42) fibril (blue-orange cartoon-surface representation). (B and C) Predominant CR binding pose (sphere representation) from the c3 cluster in side (B) and top-view (C), with amino acids (cyan ball-stick model) binding CR.

THT's binding site is easily accessible,[34] which holds true for the predicted site. Studies also suggest a minimal THT binding site on the fibril surface that covers four consecutive β-strands,[25,26] a feature we also identified (Fig. 1B and C). THT binds to Aβ fibrils but does not bind to monomers or other oligomeric states,[34] supporting the view that multiple β-strands are involved in THT binding. In the case of amyloid spherulites, THT binds with its long axis almost in parallel to the long axis of the spherulites.[35] This orientation was also observed in an X-ray structure of THT attached to a PSAM ladder,[25] during MD simulations of THT binding to a protofilament,[15] and herein (Fig. 1B and C). Finally, previous studies suggested that THT binds to hydrophobic channels formed by adjacent side chains along the long axis of amyloid fibrils.[35] By contrast, the X-ray structure of THT attached to a PSAM ladder suggested that THT binds on surfaces formed by tyrosine residues,[25] which align in a V-shaped orientation,[25] similar to the orientation of F20 found here (Fig. 1B and C). In contrast to a previous study suggesting multiple binding sites for THT to Aβ(1–42) with different binding affinities,[36] during our MD simulations, THT binds exclusively to one site with similar affinity. However, no structural information is available that characterizes the previously proposed binding sites.[36] As the structure of Aβ(1–42) fibrils strongly depends on the experimental conditions,[16,37,38] the deviation with the previous study may arise from a different fibril structure.[16] Note that our binding model still allows the binding of multiple THT molecules, as the number of binding sites increases with fibril size.

CR is predicted to bind to a hydrophobic channel formed by Y10, E11, and V12. Two structural features are essential for CR binding to Aβ aggregates: first, two negative charges separated by ~19 Å[10] and, second, a biaryl core framework.[10] Modifying the gap between the negative charges reduces the binding affinity,[10] but modifying the substituents of the biaryl core barely influences the binding affinity.[10,39] The spacing of ~19 Å corresponds to the spacing of five pleated and stacked β-strands,[11,16] suggesting that CR binds across multiple layers, thereby forming ionic interactions. CR was shown to bind to the surface of stacked β-strands, that way creating ionic interactions between the sulfonic groups of CR and lysine residues of the HET fibril.[40] As the CR molecule considered in our simulations, however, does not carry two negatively charged groups (Fig. S1B, ESI†), it is not surprising that we did not observe the ionic interaction model. Still, we find that CR binds to the surface of stacked β-strands (Fig. 2B and C). In our case, however, CR forms mainly hydrophobic contacts, which may be explained by a suggested second binding site for CR-type ligands,[10] for which the importance of hydrophobic interactions for CR binding has been stressed.[11,15,41] By contrast, some experimental results cannot be explained by the ionic model.[10] Interestingly, for CR derivatives where no ionic state is expected at physiological pH, the binding affinity increased relative to CR,[10] supporting the view that hydrophobic interactions are crucial for CR binding. The affinity of CR-like probes also decreases significantly after replacing the amino by hydroxyl groups,[10] which is surprising at first sight, as amino and hydroxyl groups both are hydrogen bond acceptor and donor groups. As observed for other azo dyes,[42,43] a hydroxyl group in the *ortho* position relative to the azo group implements azo-hydrazone tautomerism, a feature that must be considered during evaluations of the experiments.[10] Interestingly, in our model, the amino groups form hydrogen bonds with the carbonyl oxygen of E11, and the same stabilizing interactions were also observed for CR binding to HET fibrils.[40] Finally, most studies suggest that CR binds with its long axis perpendicular to the direction of the β-strands,[11,44] as shown herein (Fig. 2B and C).

We corroborated the binding modes by comparing K_D^{comp} with available K_D^{exp}, which are in good agreement; note that, to our knowledge, binding affinities of the probes to the recently resolved Aβ(1–42) fibril structure at pH 2 have not yet been determined.[16] Besides the Aβ(1–42) fibril structure obtained at pH 2 used here, other Aβ structures provide further evidence for two symmetrically arranged stacks of Aβ peptides.[37,45–47]

Throughout the simulations, the fibril preserved its structural organization, and dye binding has no significant influence on the fibril structure (Fig. S9, ESI†), although minor structural changes were observed at the fibril ends (see Movie S2, ESI† after 37 s). Changing the pH may be of relevance for THT, as the

affinity to insulin and HET fibrils decreases at acidic pH conditions, suggesting a pH dependency of THT binding.[11,48] As to CR, there is no evidence suggesting a pH dependency, although most of the affinity studies are done at neutral pH.[48]

In conclusion, we present binding sites and modes for THT and CR to the Aβ(1–42) fibril. Binding sites, modes, and affinities agree with previous experimental observations. The insights provide a starting point for the systematic search and design of novel probes that bind to Aβ(1–42) fibrils, which is essential for conclusively diagnosing Aβ(1–42) fibrils-related diseases.

We are grateful for computational support and infrastructure provided by the ''Zentrum für Informations- und Medientechnologie'' (ZIM) at the Heinrich Heine University Düsseldorf and the computing time provided by the John von Neumann Institute for Computing (NIC) to H. G. on the supercomputer JUWELS at Jülich Supercomputing Centre (JSC, user ID: HKF7). The study was funded by internal funds of Forschungszentrum Jülich to H. G. (grant no.: HKF7).

Conflicts of interest

There are no conflicts to declare.

Notes and references

1 J. Wang, B. J. Gu, C. L. Masters and Y. J. Wang, *Nat. Rev. Neurol.*, 2017, **13**, 612–623.
2 P. Scheltens, K. Blennow, M. M. B. Breteler, B. de Strooper, G. B. Frisoni, S. Salloway and W. M. Van der Flier, *Lancet*, 2016, **388**, 505–517.
3 C. L. Masters, R. Bateman, K. Blennow, C. C. Rowe, R. A. Sperling and J. L. Cummings, *Nat. Rev. Dis. Primers*, 2015, **1**, 1–18.
4 H. V. Vinters, *Annu. Rev. Pathol.: Mech. Dis.*, 2015, **10**, 291–319.
5 A. s. Association®, 2019 Alzheimer's disease facts and figures, 2019.
6 A. s. D. International, World Alzheimer Report 2018; The state of the art of dementia research: New frontiers, 2018.
7 D. J. Selkoe and J. Hardy, *EMBO Mol. Med.*, 2016, **8**, 595–608.
8 M. Goedert, F. Clavaguera and M. Tolnay, *Trends Neurosci.*, 2010, **33**, 317–325.
9 M. Jucker and L. C. Walker, *Nature*, 2013, **501**, 45–51.
10 L. S. Cai, R. B. Innis and V. W. Pike, *Curr. Med. Chem.*, 2007, **14**, 19–52.
11 M. Groenning, *J. Chem. Biol.*, 2010, **3**, 1–18.
12 A. I. Sulatskaya, I. M. Kuznetsova and K. K. Turoverov, *J. Phys. Chem. B*, 2011, **115**, 11519–11524.
13 C. Xue, T. Y. W. Lin, D. Chang and Z. F. Guo, *R. Soc. Open Sci.*, 2017, **4**, 160696.
14 E. I. Yakupova, L. G. Bobyleva, I. M. Vikhlyantsev and A. G. Bobylev, *Biosci. Rep.*, 2019, **39**, BSR20181415.
15 C. Wu, Z. X. Wang, H. X. Lei, W. Zhang and Y. Duan, *J. Am. Chem. Soc.*, 2007, **129**, 1225–1232.
16 L. Gremer, D. Schölzel, C. Schenk, E. Reinartz, J. Labahn, R. B. G. Ravelli, M. Tusche, C. Lopez-Iglesias, W. Hoyer, H. Heise, D. Willbold and G. F. Schröder, *Science*, 2017, **358**, 116–119.
17 B. R. Miller, T. D. McGee, J. M. Swails, N. Homeyer, H. Gohlke and A. E. Roitberg, *J. Chem. Theory Comput.*, 2012, **8**, 3314–3321.
18 D. A. McQuarrie, *Statistical mechanics*, University Science Books, 2000.
19 H. Y. Sun, L. L. Duan, F. Chen, H. Liu, Z. Wang, P. C. Pan, F. Zhu, J. Z. H. Zhang and T. J. Hou, *Phys. Chem. Chem. Phys.*, 2018, **20**, 14450–14460.
20 H. Gohlke and D. A. Case, *J. Comput. Chem.*, 2004, **25**, 238–250.
21 Z. Cournia, B. Allen and W. Sherman, *J. Chem. Inf. Model.*, 2017, **57**, 2911–2937.
22 J. Zhang, A. Sandberg, A. Konsmo, X. Y. Wu, S. Nystrom, K. P. R. Nilsson, P. Konradsson, H. LeVine, M. Lindgren and P. Hammarstrom, *Chem. – Eur. J.*, 2018, **24**, 7210–7216.
23 Z. P. Zhuang, M. P. Kung, C. Hou, D. M. Skovronsky, T. L. Gur, K. Plossl, J. Q. Trojanowski, V. M. Y. Lee and H. F. Kung, *J. Med. Chem.*, 2001, **44**, 1905–1914.
24 A. I. Sulatskaya, A. A. Maskevich, I. M. Kuznetsova, V. N. Uversky and K. K. Turoverov, *PLoS One*, 2010, **5**, e15385.
25 M. Biancalana, K. Makabe, A. Koide and S. Koide, *J. Mol. Biol.*, 2009, **385**, 1052–1063.
26 C. Wu, M. Biancalana, S. Koide and J. E. Shea, *J. Mol. Biol.*, 2009, **394**, 627–633.
27 M. Stravalaci, M. Beeg, M. Salmona and M. Gobbi, *Biosens. Bioelectron.*, 2011, **26**, 2772–2775.
28 W. E. Klunk, J. W. Pettegrew and D. J. Abraham, *J. Histochem. Cytochem.*, 1989, **37**, 1273–1281.
29 M. G. Iadanza, R. Silvers, J. Boardman, H. I. Smith, T. K. Karamanos, G. T. Debelouchina, Y. C. Su, R. G. Griffin, N. A. Ranson and S. E. Radford, *Nat. Commun.*, 2018, **9**, 4517.
30 B. S. Li, P. Ge, K. A. Murray, P. Sheth, M. Zhang, G. Nair, M. R. Sawaya, W. S. Shin, D. R. Boyer, S. L. Ye, D. S. Eisenberg, Z. H. Zhou and L. Jiang, *Nat. Commun.*, 2018, **9**, 3609.
31 R. Guerrero-Ferreira, N. M. I. Taylor, D. Mona, P. Ringler, M. E. Lauer, R. Riek, M. Britschgi and H. Stahlberg, *eLife*, 2018, **7**, e36402.
32 C. Röder, N. Vettore, L. N. Mangels, L. Gremer, R. B. Rayelli, D. Willbold, W. Hoyer, A. K. Buell and G. F. Schröder, *Nat. Commun.*, 2019, **10**, 3754.
33 C. König, R. Skanberg, I. Hotz, A. Ynnerman, P. Norman and M. Linares, *Chem. Commun.*, 2018, **54**, 3030–3033.
34 H. LeVine, *Arch. Biochem. Biophys.*, 1997, **342**, 306–316.
35 M. R. H. Krebs, E. H. C. Bromley and A. M. Donald, *J. Struct. Biol.*, 2005, **149**, 30–37.
36 I. M. Kuznetsova, A. I. Sulatskaya, V. N. Uversky and K. K. Turoverov, *Mol. Neurobiol.*, 2012, **45**, 488–498.
37 M. T. Colvin, R. Silvers, Q. Z. Ni, T. V. Can, I. Sergeyev, M. Rosay, K. J. Donovan, B. Michael, J. Wall, S. Linse and R. G. Griffin, *J. Am. Chem. Soc.*, 2016, **138**, 9663–9674.
38 Y. L. Xiao, B. Y. Ma, D. McElheny, S. Parthasarathy, F. Long, M. Hoshi, R. Nussinov and Y. Ishii, *Nat. Struct. Mol. Biol.*, 2015, **22**, 499–504.
39 W. Zhen, H. Han, M. Anguiano, C. A. Lemere, C. G. Cho and P. T. Lansbury, *J. Med. Chem.*, 1999, **42**, 2805–2815.
40 A. K. Schütz, A. Soragni, S. Hornemann, A. Aguzzi, M. Ernst, A. Bockmann and B. H. Meier, *Angew. Chem., Int. Ed.*, 2011, **50**, 5956–5960.
41 J. H. Cooper, *Lab. Invest.*, 1974, **31**, 232–238.
42 A. S. Ozen, P. Doruker and V. Aviyente, *J. Phys. Chem. A*, 2007, **111**, 13506–13514.
43 H. Zollinger, *Color chemistry: syntheses, properties, and applications of organic dyes and pigments*, John Wiley & Sons, 2003.
44 L. W. Jin, K. A. Claborn, M. Kurimoto, M. A. Geday, I. Maezawa, F. Sohraby, M. Estrada, W. Kaminsky and B. Kahr, *Proc. Natl. Acad. Sci. U. S. A.*, 2003, **100**, 15294–15298.
45 M. Kollmer, W. Close, L. Funk, J. Rasmussen, A. Bsoul, A. Schierhorn, M. Schmidt, C. J. Sigurdson, M. Jucker and M. Fändrich, *Nat. Commun.*, 2019, **10**, 4760.
46 M. A. Wälti, F. Ravotti, H. Arai, C. G. Glabe, J. S. Wall, A. Böckmann, P. Güntert, B. H. Meier and R. Riek, *Proc. Natl. Acad. Sci. U. S. A.*, 2016, **113**, E4976–E4984.
47 A. K. Schütz, T. Vagt, M. Huber, O. Y. Ovchinnikova, R. Cadalbert, J. Wall, P. Güntert, A. Böckmann, R. Glockshuber and B. H. Meier, *Angew. Chem., Int. Ed.*, 2015, **54**, 331–335.
48 M. Groenning, M. Norrman, J. M. Flink, M. van de Weert, J. T. Bukrinsky, G. Schluckebier and S. Frokjaer, *J. Struct. Biol.*, 2007, **159**, 483–497.

